BIOTECHNOLOGY

# Genetically targeted chemical assembly of functional materials in living cells, tissues, and animals

Jia Liu[1]*, Yoon Seok Kim[2]*, Claire E. Richardson[3]*, Ariane Tom[2]*, Charu Ramakrishnan[2], Fikri Birey[4], Toru Katsumata[1], Shucheng Chen[1], Cheng Wang[5], Xiao Wang[2], Lydia-Marie Joubert[6], Yuanwen Jiang[1], Huiliang Wang[2], Lief E. Fenno[2,4], Jeffrey B.-H. Tok[1], Sergiu P. Paşca[4], Kang Shen[3,7], Zhenan Bao[1]†, Karl Deisseroth[2,4,7]†

The structural and functional complexity of multicellular biological systems, such as the brain, are beyond the reach of human design or assembly capabilities. Cells in living organisms may be recruited to construct synthetic materials or structures if treated as anatomically defined compartments for specific chemistry, harnessing biology for the assembly of complex functional structures. By integrating engineered-enzyme targeting and polymer chemistry, we genetically instructed specific living neurons to guide chemical synthesis of electrically functional (conductive or insulating) polymers at the plasma membrane. Electrophysiological and behavioral analyses confirmed that rationally designed, genetically targeted assembly of functional polymers not only preserved neuronal viability but also achieved remodeling of membrane properties and modulated cell type–specific behaviors in freely moving animals. This approach may enable the creation of diverse, complex, and functional structures and materials within living systems.

The complex properties of living systems arise from the structure and function of constituent cells, exemplified by the roles of neurons (*1*) within nervous systems (*2*, *3*). We considered whether specific cells within intact biological systems may be genetically co-opted to build new physical structures with desired form and function. Incorporation of miniaturized electrical components onto membranes can change cellular activity (*4*–*6*), although without the capability for genetic targeting of cells. In another approach, electroactive (such as conductive) polymers have been directly synthesized through electrochemical polymerization in living tissue to reduce impedance (*7*), although without the genetic targeting of cells or cell types.

To achieve biocompatible in vivo synthesis of electroactive polymers within genetically specified cells of living animals, we began with conductive polymers from polyaniline (PANI) and poly(3,4-ethylenedioxythiophene) (PEDOT). These polymers were chosen for aqueous synthesis (which is important for biological system compatibility) and for dual conduction of electrons and ions, which reduces local electrochemical impedance (*8*) when interfacing electronics with living cells. We designed a single-enzyme–facilitated polymerization using chemically modified monomers (Fig. 1A) for which polymerization is triggered by an enzyme that can be expressed in specific cells. Perfusion of small-molecule conductive-polymer precursors capable of diffusion through intact tissue (step I) was followed by oxidative radical cation polymerization steps at the genetically targeted

[1]Department of Chemical Engineering, Stanford University, Stanford, CA 94305, USA. [2]Department of Bioengineering, Stanford University, Stanford, CA 94305, USA. [3]Department of Biology, Stanford University, Stanford, CA 94305, USA. [4]Department of Psychiatry, Stanford University, Stanford, CA 94305, USA. [5]Advanced Light Source, Lawrence Berkeley National Laboratory, Berkeley CA 94720, USA. [6]Cell Sciences Imaging Facility, Stanford University, Stanford, CA 94305, USA. [7]Howard Hughes Medical Institute, Stanford University, Stanford, CA 94305, USA.
*These authors contributed equally to this work.
†Corresponding author. Email: deissero@stanford.edu (K.D.); zbao@stanford.edu (Z.B.)

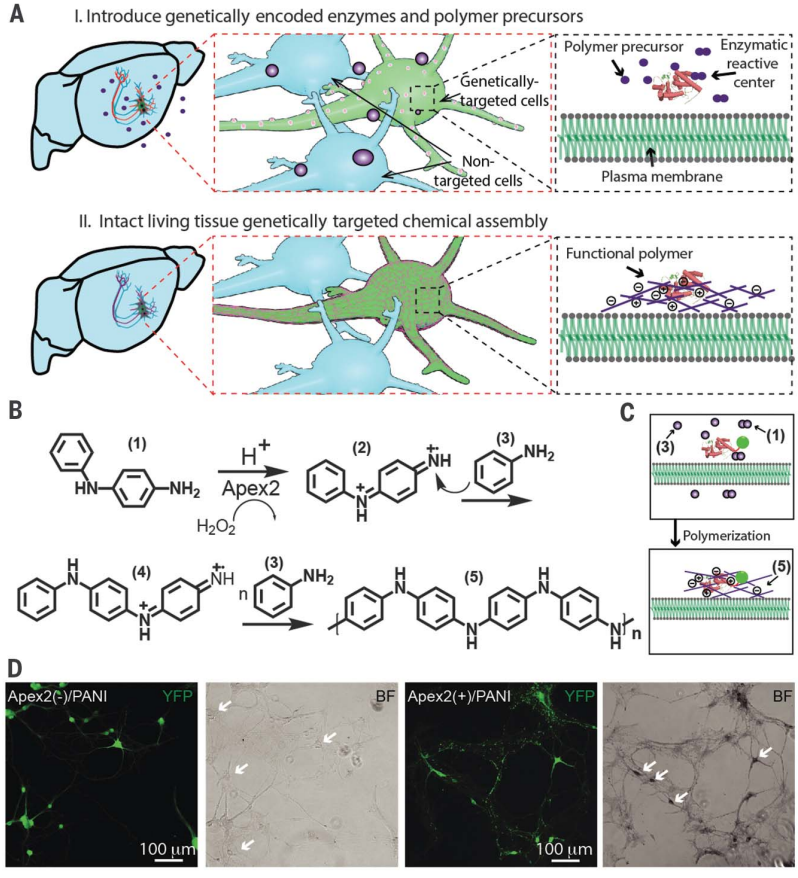


**Fig. 1. Genetically targeted chemical assembly of functional materials in cells.** (**A**) Specific instantiation shown is enzyme/$H_2O_2$–catalyzed functional polymerization in brain. Blue indicates non–enzyme-targeted cells. (**B**) Reaction of Apex2-mediated polymerization from precursor reagents containing aniline monomer-dimer mixture. Labels 1 to 5 show chemical structures of N-phenylenediamine (aniline dimer, **1**), aniline dimer radical cations (**2**), aniline monomer (**3**), aniline trimer radical cations (**4**), and polyaniline (PANI, **5**), respectively. (**C**) Schematic of Apex2-mediated polymerization and deposition of PANI on targeted cells. (**D**) In situ genetically targeted synthesis and incorporation of conductive polymer. Shown are epifluorescence (YFP) and BF images of fixed rat hippocampal neurons. Arrows indicate individual neurons.

enzyme's reactive center. Because of the short mean diffusion length of radical cations in aqueous solution and low solubility of the resulting polymers, the synthesized conductive polymers were expected to be deposited onto targeted cells at juxtamembranous locations (a design feature for limiting adverse effects on native intracellular chemistry) (step II).

Peroxidases can catalyze synthesis of conductive polymers in the presence of hydrogen peroxide ($H_2O_2$) in vitro under harsh conditions: high concentrations of hydrogen peroxide (>1 mM), low pH (pH = 1 to 5), and high monomer concentrations (>10 mM) (*9*). Therefore, we sought a biocompatible synthesis by enabling polymerization in pH-neutral and biocompatible conditions. We first expressed a humanized version of ascorbate peroxidase Apex2 (*10*); cultured rat hippocampal neurons were transduced with adeno-associated virus (AAV) vectors containing Apex2 and in some cases fused with a 13–amino acid peptide (selected in a screen for expression-enhancing tags) (fig. S1) (*11*) and/or enhanced yellow fluorescent protein (YFP) (for tracking localization) (Fig. 1A). We first selected aniline as the monomer for its relatively low oxidation potential (*12*), but Apex2 was unable to polymerize aniline monomers in phosphate-buffered saline (fig. S2A). Because *N*-phenylenediamine (an aniline dimer) would further reduce oxidation potential (*13*), an aniline monomer-dimer mixture (0.5 mM, 1:1 molar ratio) (Fig. 1B) was added to an aqueous solution of 0.1 mM $H_2O_2$ and applied to fixed cultured neurons (Fig. 1C). Epifluorescence and bright-field (BF) phase images confirmed that Apex2(+) but not Apex2(−) neurons exhibited a dark-colored reaction product (Fig. 1D and fig. S2, B and C). Confocal images revealed a formation of deposited aggregates (fig. S3).

To test whether these deposits consisted of PANI, we used ultraviolet-visible–near infrared (UV-vis-NIR) absorption spectroscopy to compare with spectra previously reported for PANIs (Fig. 2A). The shorter absorption peak wavelength of Apex2(+)/PANI (~574 nm versus ~620 nm for commercial 50 kDa PANI) indicated that the synthesized polymer was of lower molecular weight (Fig. 2B). We then treated the PANI-fixed neurons with 100 mM *p*-toluenesulfonic acid (termed Apex2(+)/dPANI), which resulted in increased conductivity and red-shift in the UV-vis spectrum (Fig. 2A), as expected for doped PANI (*14*). For Apex2(−)/PANI, Apex2(+)/PANI, and Apex2(+)/dPANI neurons, we observed expected color changes (fig. S4A). The UV-vis-NIR spectrum showed a red-shifted peak at ~615 nm for doped PANI (Fig. 2C), indicating transition to the emeraldine salt form (*14*). Peak absorption-wavelength was maintained across different reaction times, suggesting increased PANI deposition over time (fig. S4, B and C). X-ray photoelectron spectroscopy (XPS) showed enhanced S-element signal only in Apex2(+)/

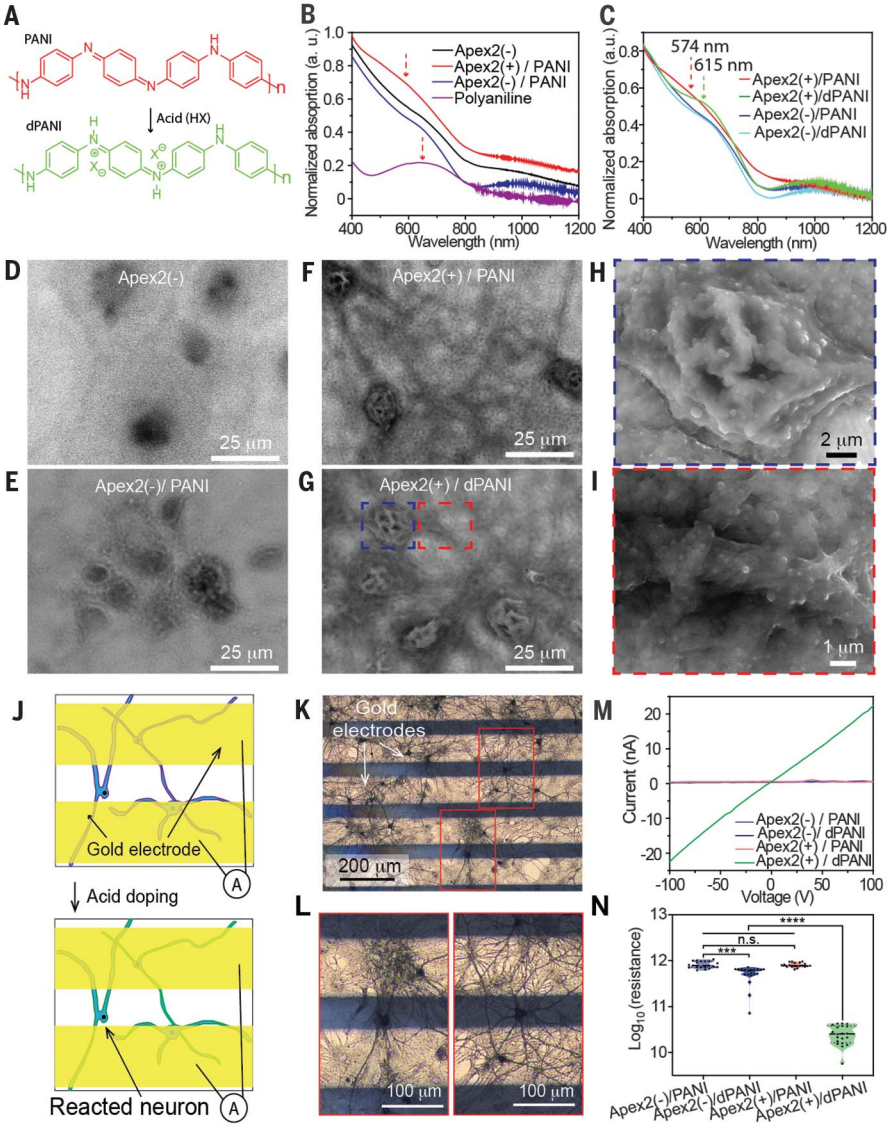


**Fig. 2. Chemical and electrical characterization of synthesized conductive polymer.**
(**A**) Structures shown are PANI (red) conversion to doped PANI (dPANI, green), by means of acid (HX) treatment. (**B**) Normalized UV-vis-NIR spectra. Pure PANI, purple; Apex2(−) neurons black; Apex2(−)/PANI neurons, blue; and Apex2(+)/PANI neurons, red. Arrows indicate absorption peak. (**C**) UV-vis-NIR spectra of Apex2(−)/PANI and Apex2(+)/PANI before and after *p*-toluenesulfonic acid treatment. Dashed arrows indicate red-shift of absorption peak in UV-vis from ~574 to ~615 nm. (**D** to **I**) Variable-pressure SEM images of (D) nonreacted wild-type, (E) Apex2(−)/PANI, (F) Apex2(+)/PANI, and (G) Apex2(+)/dPANI neurons. Zoomed-in images of (H) blue- and (I) red-boxed regions from (G) show polymer deposition. (**J**) Schematic of electrical interface to fixed neurons (blue) with PANI coating, for conductivity measurements. Acid doping (green) was used to test presence of deposited conductive polymer. (**K** and **L**) BF image of postreacted neurons on the glass substrate with gold electrodes for current-voltage (*I-V*) measurement. (**M** and **N**) Representative *I-V* curves (M) and summary of resistance changes (N) (log-scale violin plots of resistance, $n = 20$ electrode-pairs per category, $^{***}P < 0.001$, $^{****}P < 0.0001$, unpaired two-tailed $t$ test) between electrodes for cultured Apex2(−) and Apex2(+) neurons on slides before and after acidic vapor treatment (HCl). Reduction in Apex2(−)/dPANI sample likely because of ionic conductivity from evaporated HCl solution.

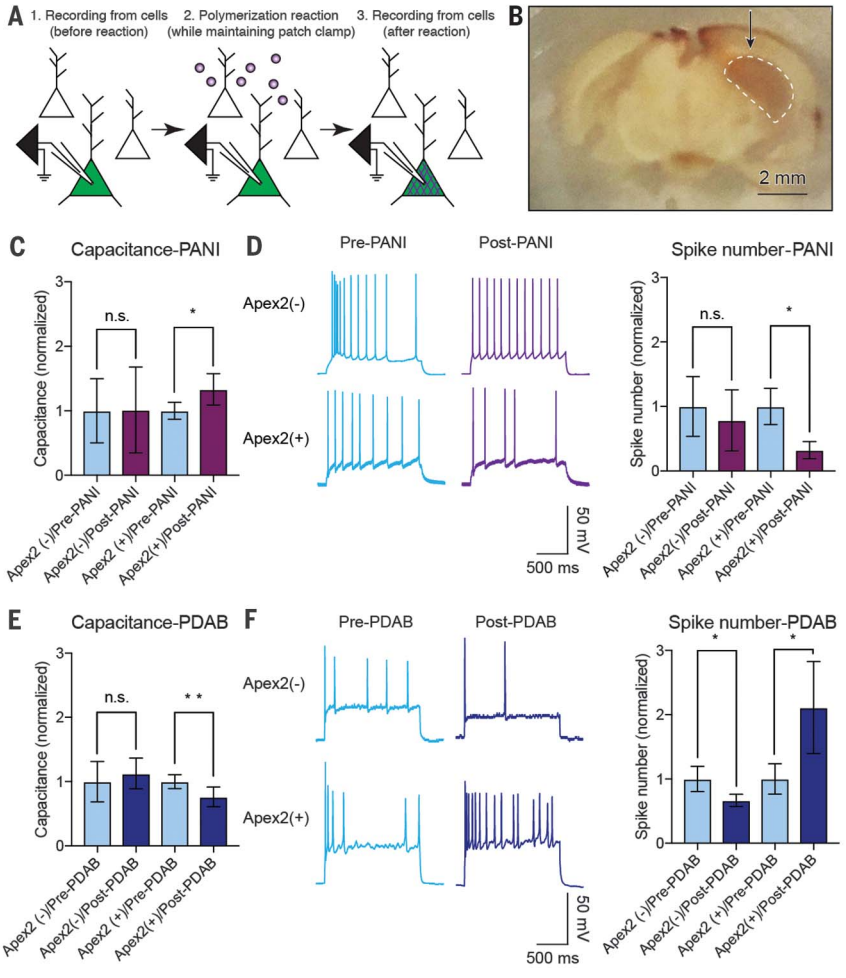


**Fig. 3. Electrophysiological characterization: conductive polymers in living brain slices.** Light blue, before reaction; purple, after PANI; dark blue, after PDAB. (**A**) Slice physiology workflow. (**B**) Photomicrograph of brain slice after polymerization reaction. Arrow indicates injection site of Apex2 virus; dashed line indicates hippocampus. (**C**) Membrane capacitance and (**D**) current-injection–evoked spikes before and after PANI polymerization [mean ± SEM, $n$ = 7 Apex2(+) conditions, (C) $n$ = 4 Apex2(−), (D) $n$ = 3 Apex2(−); all individual cells were maintained in the whole-cell patch clamp configuration across pre-reaction and post-reaction time points for direct comparison; ratio-paired $t$ tests: $^*P < 0.05$]. All postconditions here and in (E) and (F) were normalized to corresponding preconditions for comparison; mean capacitance values were 20 to 45 pF. (**E**) Membrane capacitance and (**F**) current-injection–evoked spikes before and after PDAB polymerization. Increased spiking can be seen with Apex2(+)/PDAB despite mild rundown from PDAB-only Apex2(−) reaction conditions [mean ± SEM, (E) $n$ = 10 Apex2(+), (F) $n$ = 8 Apex2(+), (E) $n$ = 5 Apex2(−), (F) $n$ = 4 Apex2(−). Ratio-paired $t$ tests: $^*P < 0.05$, $^{**}P < 0.01$].

dPANI neurons, confirming incorporation of *p*-toluenesulfonic acid (fig. S5A). Near-edge x-ray absorption fine structure (NEXAFS), for identifying different types of C–N or C=N features from amines and imines (*15*), confirmed the chemical composition of the deposited material (fig. S5, C to G).

Variable-pressure scanning electron microscopy (VP-SEM) imaging of neurons provided initial qualitative comparison of conductivity before and after reaction (Fig. 2, D to G, and fig. S6). Apex2(+)/PANI neurons in liquid showed higher contrast, which is consistent with a more conductive outer layer (Fig. 2F), with contrast further enhanced through acidic doping (Fig. 2G). Both soma and neurites could be directly observed, suggesting substantial surface-conductivity enhancement (*16*) from doped PANI (Fig. 2, H and I). In addition, transmission electron microscopy (TEM) confirmed deposition of polymers on neuronal membranes (fig. S7).

We further investigated the conductive nature of PANI-fixed neurons by depositing gold electrodes onto air-dried, fixed neurons (Fig. 2, J to L); electrical conduction between electrodes was expected to only arise from conductive polymer on the neurons. To prevent delamination between gold electrodes and polymers during solution-doping, HCl vapor was used to dope the polymer. Apex2(+)/dPANI showed the lowest resistance, as expected (Fig. 2, M and N). We tested other polymers, including a poly(3,4-ethylenedioxythiophene/PEDOT) derivative, sodium 4-((5,7-di(thiophen-2-yl)-2,3-dihydrothieno[3,4-b][1,4]dioxin-2-yl)methoxy)butane-1-sulfonate (termed TETs) (*17*), and a nonconductive polymer, poly(3,3′-diaminobenzidine) (PDAB) (*18*). Apex2(+)/PANI-PTETs neurons showed higher conductivity than that of Apex2(−)/PANI-PTETs neurons (fig. S8), whereas Apex2(+)/PDAB showed no conductivity change compared with that of Apex2(−)/PDAB (fig. S9). To further verify conductivity, we cultured human embryonic kidney 293T cells in a confluent sheet suited for conductivity measurements (fig. S10). Apex2(+)/PANI without acidic doping exhibited an approximately two orders of magnitude reduction in resistance versus that of Apex2(−)/PANI control. We next investigated Apex2-catalyzed polymerization in human cortical spheroids (hCS), a human stem cell–derived three-dimensional (3D) organoid (*19*, *20*). We observed coloration (fig. S11A) and particle deposits within 30 min of reaction-treated Apex2(+)/PANI hCS at locations corresponding to YFP signal (fig. S11, B to E). In another 3D preparation (brain slices), the dark-colored reaction product could be visualized ~60 μm and 110 μm deep after 30- and 60-min reactions, respectively (fig. S12).

We further explored application of this method to living systems. Neurons remained viable after exposure to the aniline and its dimer in 0.05 mM $H_2O_2$ (fig. S15A)—a reaction condition sufficient for polymer deposition (fig. S13, A and B) [verified by means of UV-vis-NIR absorption (fig. S13, C to E)]. The same reaction condition in living mice elicited no reactive gliosis over weeks (fig. S14). We also performed whole-cell patch clamp in Apex2(+)- and Apex2(−)-cultured rat hippocampal neurons before and after PANI or PDAB polymerization (fig. S15). Current injection in Apex2(+)/PDAB neurons elicited robust action potentials both before and after polymerization, decreased capacitance consistent with the expected juxtamembranous localization of this insulating polymer, and increased charge-separation distance across the membrane; by contrast, Apex2(+)/PANI neurons showed decreased action-potential firing with increased capacitance (fig. S15, B to I), which is consistent

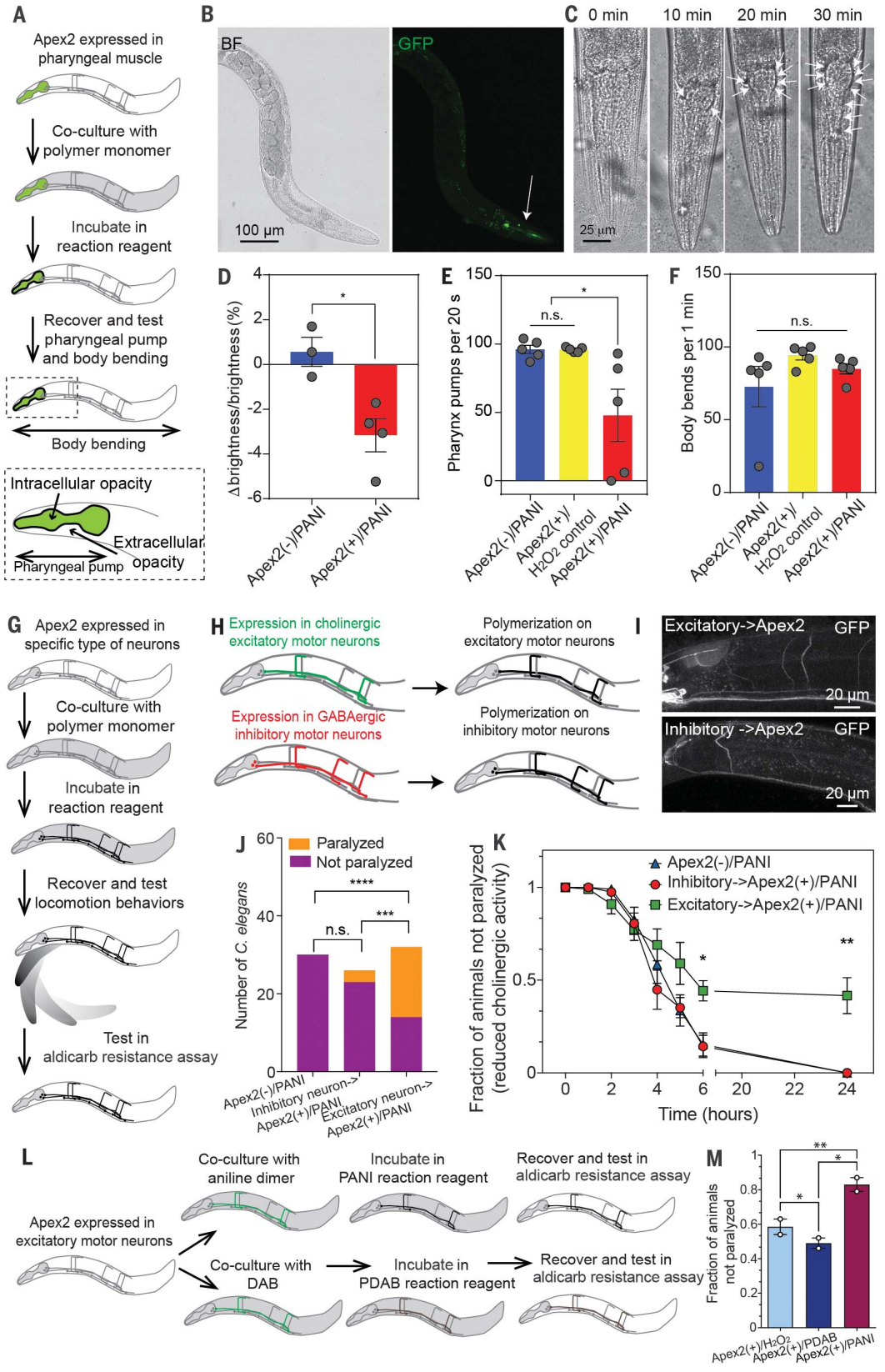


**Fig. 4. Cell type–specific polymerization in *C. elegans*.** (**A**) Schematic of targeting polymerization to pharyngeal muscle. (**B**) BF (left) and fluorescence images (right) of *C. elegans* expressing *Pmyo-2::Apex2::mcd8::gfp* labeled Apex2(+) versus wild-type controls labeled Apex2(−). Arrow indicates GFP-labeled pharyngeal muscle and Apex2 expression. (**C**) BF time-course images of pharyngeal muscle of Apex2(+) worms in 30-min PANI reaction. Arrows indicate increased black reaction-product in Apex2(+) between pharyngeal muscle and epidermis. (**D**) Brightness change. Shown is Apex2(−) versus Apex2(+) after reaction (mean ± SEM, $n$ = 3 to 4 animals, $^*P < 0.05$, two-tailed, unpaired $t$ test). (**E**) Body-bending rate and (**F**) pharyngeal-pumping rate for Apex2(−)/PANI, Apex2(+)/$H_2O_2$ control, and Apex2(+)/ polymerization (mean ± SEM, $^*P < 0.05$, $n$ = 5 animals each condition, two-tailed unpaired $t$ test). (**G**) Schematic of motor-neuron testing. (**H**) Cell type–specific polymerization of GABAergic (inhibitory) neurons [Inhibitory→Apex2(+)] or cholinergic (excitatory) neurons [Excitatory→Apex2(+)]. Black lines indicate cell type–specific polymer. (**I**) Inhibitory→Apex2(+) (top) or Excitatory→Apex2(+) (bottom) motor neurons expressing *Apex2::mcd8::gfp* under *Punc-47* or *Punc-17* promoters, respectively. (**J**) Excitatory→Apex2(+) worms show reduced locomotion after polymerization, whereas Inhibitory→Apex2(+) worms show negligible paralysis. ($n$ = 30 animals for Apex2(−), $n$ = 26 animals for Inhibitory→Apex2(+), and $n$ = 32 animals for Excitatory→Apex2(+); $^{***}P < 0.001$, $^{****}P < 0.0001$, one-sided Fisher's exact test). (**K**) Aldicarb resistance assay after polymerization [50 animals per strain, two replicates, one-way analysis of variance (ANOVA)/Tukey correction, $^*P < 0.05$, $^{**}P < 0.01$]. (**L**) Schematic of polymerization of conductive (PANI) and insulating (PDAB) polymers in worm cholinergic motor neurons. (**M**) Summary of fraction-resistant *C. elegans* after 5 hours in aldicarb resistance assay (mean ± SEM, $^*P < 0.05$, $^{**}P < 0.01$, one-way ANOVA test, Tukey correction).

with reported capacitance effects resulting from conducting-polymer introduction (*21*, *22*).

To allow rigorous testing of the same cells before and after polymerization, we also conducted recordings in acute brain slices (Fig. 3A), which allowed holding the same cells in whole-cell patch clamp throughout the polymerization reaction. Four weeks after Apex2 virus injection, we observed robust Apex2-driven polymerization (Fig. 3B and fig. S12), with increased capacitance after PANI reaction and decreased capacitance after PDAB reaction (Fig. 3, C and E). Little effect was observed on other passive membrane properties (fig. S16), and patched cells were healthy in terms of input resistance and resting potential under all conditions. We next studied action potentials (Fig. 3, D and F); whereas Apex2(−) neuron firing rates were unchanged after treatment, Apex2(+)/PANI neurons exhibited decreased current-injection–evoked firing, and Apex2(+)/PDAB neurons showed increased firing (Fig. 3, D and F). The stability of resting potential and input resistance coupled with the bidirectionality of this effect would not have been expected from non-specific cell-health mechanisms for altered firing. By contrast, experimental and theoretical studies have demonstrated an inverse correlation between spike firing and capacitance (supplementary materials) (*23*–*25*), which is consistent with our slice physiology that shows increased capacitance after conductive-polymer deposition on the dielectric lipid bilayers of living neurons and decreased capacitance after insulating-polymer deposition (Fig. 3, C and E).

Last, we tested behavior in freely moving animals upon assembling genetically targeted electroactive polymers in vivo. We expressed Apex2–green fluorescent protein (GFP) on the membrane of worm (*Caenorhabditis elegans*) pharyngeal muscle cells (Fig. 4, A and B) and observed robust localized polymerization (Fig. 4, C and D, and fig. S18, A and B). Apex2(+)/PANI worms exhibited reduced pumping frequency of pharyngeal muscle (Fig. 4E) consistent with the inhibition of targeted cells observed in cultured neuron and brain slice electrophysiology, but no quantitative alteration in other body movements, such as bending (Fig. 4F). Because liquid-state atomic force microscopy showed no clear changes in Young's modulus of cellular membranes after polymerization (fig. S17), altered pharyngeal pumping was unlikely owing to changed elasticity of muscle membranes, and viability assays confirmed long-term biocompatibility of PANI in worms (fig. S18, A and C).

We next expressed Apex2-GFP in γ-aminobutyric acid (GABA)–ergic (inhibitory) or cholinergic (excitatory) motor neurons (Fig. 4, G to I, Inhibitory→Apex2(+) and Excitatory→Apex2(+), respectively). After polymerization (Fig. 4J), Excitatory→Apex2(+)/PANI worms displayed impaired sinusoidal forward locomotion (both spontaneous and aversive-stimulus–evoked), which is concordant with prior observations from optogenetic inhibition of worm excitatory neurons (*26*). Sinusoidal forward locomotion in Apex2(−)/PANI and Inhibitory→Apex2(+)/PANI was unaffected. On the other hand, Inhibitory→Apex2(+)/PANI worms exhibited increased reversal frequency (fig. S18, D to G) and increased sharp (<90°) turns versus Apex(−)/PANI worms (fig. S18H), which is consistent with prior results from optogenetic manipulation of inhibitory neurons that also induced sharper turns (*27*). Inhibitory→Apex2(+)/PANI worms maintained the capability to move forward in sinusoidal waves of unchanged amplitude (fig. S18I) and minimally reduced wavelength (fig. S18J), but when inhibitory neurons were ablated (*unc*25-null), sinusoidal wave amplitude was greatly reduced (fig. S18, K and L) (*28*).

Consistent with this pattern, Excitatory→Apex2(+)/PANI worms became resistant to the acetylcholinesterase-inhibitor aldicarb, suggesting that this treatment causes reduced acetylcholine release, but Inhibitory→Apex2(+)/PANI and Apex2(−)/PANI worms did not (Fig. 4K and fig. S19, A and B). Moreover, Excitatory→Apex2(+)/PDAB showed reduced resistance to aldicarb, compared with Excitatory→Apex2(+)/PANI (Fig. 4, L and M, and fig. S19C), pointing to enhanced cholinergic activity with insulating-polymer assembly—a specific gain of function in living animals and an opposite-direction effect compared with conducting-polymer assembly, both of which are concordant with the electrophysiology.

We have achieved chemical assembly of electroactive polymers on genetically specified cellular elements within living cells, tissues, and animals. Future work may address potential limitations and opportunities; for example, reaction products could over time occupy substantial space in and near targeted cells, which may be useful in some contexts but also could result in cytotoxicity. Distinct strategies for the targeting and triggering of chemical synthesis could extend beyond the oxidative radical initiation shown here while building on the core principle of assembling within cells (as reaction compartments) genetically and anatomically targeted reactants (such as monomers), catalysts (such as enzymes or surfaces), or reaction conditions (through modulators of pH, light, heat, redox potential, electrochemical potential, and other chemical or energetic signals). Diverse cell-specific chemical syntheses may thus be explored and developed for a broad array of functional characteristics in assembled structures.

## REFERENCES AND NOTES


1. A. L. Hodgkin, A. F. Huxley, *J. Physiol.* **117**, 500–544 (1952).
2. K. Deisseroth, *Nat. Neurosci.* **18**, 1213–1225 (2015).
3. V. Gradinaru, J. Treweek, K. Overton, K. Deisseroth, *Annu. Rev. Biophys.* **47**, 355–376 (2018).
4. T. Dvir *et al.*, *Nat. Nanotechnol.* **6**, 720–725 (2011).
5. G. Cellot *et al.*, *Nat. Nanotechnol.* **4**, 126–133 (2009).
6. J. Niu *et al.*, *Nat. Chem.* **9**, 537–545 (2017).
7. L. Ouyang, C. L. Shaw, C. C. Kuo, A. L. Griffin, D. C. Martin, *J. Neural Eng.* **11**, 026005 (2014).
8. L. Pan *et al.*, *Proc. Natl. Acad. Sci. U.S.A.* **109**, 9287–9292 (2012).
9. R. Cruz-Silva *et al.*, *Eur. Polym. J.* **41**, 1129–1135 (2005).
10. S. S. Lam *et al.*, *Nat. Methods* **12**, 51–54 (2015).
11. T. Scherf *et al.*, *Proc. Natl. Acad. Sci. U.S.A.* **98**, 6629–6634 (2001).
12. A. S. Pavitt, E. J. Bylaska, P. G. Tratnyek, *Environ. Sci. Process. Impacts* **19**, 339–349 (2017).
13. Y. Wei *et al.*, *J. Polym. Sci. C* **28**, 81–87 (1990).
14. S. E. Moulton, P. C. Innis, L. A. P. Kane-Maguire, O. Ngamna, G. G. Wallace, *Curr. Appl. Phys.* **4**, 402–406 (2004).
15. C. Henning, K. H. Hallmeier, R. Szargan, *Synth. Met.* **92**, 161–166 (1998).
16. D. J. Stokes, *Principles and Practice of Variable Pressure/ Environmental Scanning Electron Microscopy* (John Wiley, 2008).
17. E. Stavrinidou *et al.*, *Sci. Adv.* **1**, e1501136 (2015).
18. I. E. Mulazimoglu, *Asian J. Chem.* **22**, 8203–8208 (2010).
19. A. M. Pașca *et al.*, *Nat. Methods* **12**, 671–678 (2015).
20. S. A. Sloan, J. Andersen, A. M. Pașca, F. Birey, S. P. Pașca, *Nat. Protoc.* **13**, 2062–2085 (2018).
21. R. C. Van Lehn *et al.*, *Nano Lett.* **13**, 4060–4067 (2013).
22. R. P. Carney *et al.*, *ACS Nano* **7**, 932–942 (2013).
23. M. J. Gillespie, R. B. Stein, *Brain Res.* **259**, 41–56 (1983).
24. D. K. Hartline, D. R. Colman, *Curr. Biol.* **17**, R29–R35 (2007).
25. B. Howell, L. E. Medina, W. M. Grill, *J. Neural Eng.* **12**, 056015–56015 (2015).
26. H. E. Kato *et al.*, *Nature* **561**, 349–354 (2018).
27. J. L. Donnelly *et al.*, *PLOS Biol.* **11**, e1001529 (2013).
28. S. L. McIntire, E. Jorgensen, J. Kaplan, H. R. Horvitz, *Nature* **364**, 337–341 (1993).


## ACKNOWLEDGMENTS


**Funding:** K.D. was supported by NIH and NSF. J.L. was supported by Stanford Bio-X. K.D., Z.B., and S.P.P. were supported by the Wu-Tsai Neuroscience Institute. Y.S.K. was supported by the Kwanjeong International Fellowship and Stanford Bio-X. X.W. was supported by the Life Sciences Research Foundation and the Gordon and Betty Moore Foundation. We acknowledge resources of the Advanced Light Source U.S. Department of Energy (DOE) Facility (DE-AC02-05CH11231). Part of this work was performed at the Stanford Nano Shared Facilities (SNSF), supported by NSF (ECCS-1542152). **Author contributions:** Z.B. and K.D. conceived and initiated the project with implementation by the experimental team of J.L., Y.S.K., A.T., and C.R.; K.D. and C.R. designed the Apex2 molecular strategy. J.L., C.R, A.T., and Z.B. developed the polymerization reactions. J.L. and A.T. performed UV-vis characterizations. J.L. and Y.J. performed conductivity measurements. Y.S.K., L.E.F., and J.L. performed electrophysiology. C.E.R., Y.S.K., and J.L. conducted *C. elegans* work, guided by K.S.; F.B. and S.P.P. developed hCS. T.K. synthesized the TETs monomer. S.C. and J.L. conducted XPS. C.W. and J.L. conducted NEXAFS. L.-M.J., H.W., and J.L. conducted EM imaging. X.W. optimized tissue imaging. J.L., Y.S.K., A.T., Z.B., and K.D. prepared figures and wrote the manuscript with edits from all authors. Z.B. and K.D. supervised all aspects of the work. **Competing interests:** A patent application has been filed by Stanford related to this work; all methods and protocols are freely available. **Data and materials availability:** All data are available in the manuscript or supplementary materials.


## SUPPLEMENTARY MATERIALS

science.sciencemag.org/content/367/6484/1372/suppl/DC1
Materials and Methods
Figs. S1 to S19
References (*29*–*33*)

22 June 2019; accepted 21 January 2020
10.1126/science.aay4866

Science

# Genetically targeted chemical assembly of functional materials in living cells, tissues, and animals

Jia Liu, Yoon Seok Kim, Claire E. Richardson, Ariane Tom, Charu Ramakrishnan, Fikri Birey, Toru Katsumata, Shucheng Chen, Cheng Wang, Xiao Wang, Lydia-Marie Joubert, Yuanwen Jiang, Huiliang Wang, Lief E. Fenno, Jeffrey B.-H. Tok, Sergiu P. Pasca, Kang Shen, Zhenan Bao and Karl Deisseroth

*Science* **367** (6484), 1372-1376.
DOI: 10.1126/science.aay4866

**From genetics to material to behavior**

Introducing new genes into an organism can endow new biochemical functions or change the patterns of existing functions, but extending these manipulations to structure at the tissue level is challenging. Combining genetic engineering and polymer chemistry, Liu *et al.* directly leveraged complex cellular architectures of living organisms to synthesize, fabricate, and assemble bioelectronic materials (see the Perspective by Otto and Schmidt). An engineered enzyme expressed in genetically targeted neurons synthesized conductive polymers in tissues of freely moving animals. These polymers enabled modulation of membrane properties in specific neuron populations and manipulation of behavior in living animals.

*Science*, this issue p. 1372; see also p. 1303



*Science* (print ISSN 0036-8075; online ISSN 1095-9203) is published by the American Association for the Advancement of Science, 1200 New York Avenue NW, Washington, DC 20005. The title *Science* is a registered trademark of AAAS.